Ultrasonics 54 (2014) 809–820

Contents lists available at ScienceDirect

Ultrasonics

journal homepage: www.elsevier.com/locate/ultras

A finite volume method and experimental study of a stator of a piezoelectric traveling wave rotary ultrasonic motor

V. Bolborici [a,*], F.P. Dawson [b], M.C. Pugh [c]

[a] University of Texas at El Paso, Department of Electrical and Computer Engineering, 500 W. University Ave., El Paso, TX 79968, USA
[b] University of Toronto, Department of Electrical and Computer Engineering, Toronto, ON M5S 3G4, Canada
[c] University of Toronto, Department of Mathematics, Toronto, ON M5S 2E4, Canada

ARTICLE INFO

Article history:
Received 1 May 2013
Received in revised form 9 October 2013
Accepted 12 October 2013
Available online 21 October 2013

Keywords:
Piezoelectric
Ultrasonic
Motor
Stator
Eigenfrequency

ABSTRACT

Piezoelectric traveling wave rotary ultrasonic motors are motors that generate torque by using the friction force between a piezoelectric composite ring (or disk-shaped stator) and a metallic ring (or disk-shaped rotor) when a traveling wave is excited in the stator. The motor speed is proportional to the amplitude of the traveling wave and, in order to obtain large amplitudes, the stator is excited at frequencies close to its resonance frequency. This paper presents a non-empirical partial differential equations model for the stator, which is discretized using the finite volume method. The fundamental frequency of the discretized model is computed and compared to the experimentally-measured operating frequency of the stator of Shinsei USR60 piezoelectric motor.

1. Introduction

Since the invention of the piezoelectric traveling wave rotary ultrasonic motor there have been many attempts to model the stator of the motor based on experimental results and on pure analytical concepts. In [1], the authors present an empirical equivalent circuit model for the motor of a piezoelectric traveling wave rotary ultrasonic motor. The model consists of two equivalent RLC circuits (one for each phase). The equivalent inductor represents the mass effect of the ceramic body and metal ring, the equivalent capacitance represents the spring effect of the ceramic body and metal ring, and the resistance represents the losses that occur within the ceramic body and metal ring. Simulations of the model are not presented.

In [2], an empirical equivalent circuit for the stator of a piezoelectric traveling wave rotary ultrasonic motor is presented. The equivalent circuit allows for the estimation of the motor's characteristics. The equivalent circuit takes into account the external forces applied to the stator: the normal force of the rotor against the stator and the torque-generating tangential friction force between the stator and the rotor. The motor model allows for the estimation of the motor's characteristics in two operation modes: constant voltage and constant current operation. However, the model has some limitations. For example, the model does not calculate the operating frequency of the motor; rather, it is determined experimentally and then given to the model as an input parameter. Built into the model is the fact that the amplitude of the feedback signal is proportional to the speed of the motor and that the speed drop is proportional to the applied torque, but the proportionality coefficients need to be determined experimentally.

In [3,4], the authors present an enhanced empirical equivalent circuit model of a piezoelectric traveling wave rotary ultrasonic motor. The paper highlights the importance of the electromechanical coupling factor responsible for the energy conversion in the motor. Also, the model includes the effect of temperature on the mechanical resonance frequency; this effect is important for motors that operate for a long period of time. Simulations of the model show agreement with experimental measurements in the range of torques and frequencies of interest.

A drawback of empirical approaches is that such models must be developed in conjunction with experiments on the system of interest. And so a question about an operating regime that is outside the regime of the original experiments (and hence of the model) must be studied experimentally rather than with the model. In contrast, "first principles" models allow for computer explorations of a wide operating regime. These explorations can then be validated against experiment.

One type of first principles model uses Hamilton's principle. For example, the model in [5] uses the constitutive equations of piezoelectricity, Hamilton's principle, the strain–displacement relations,

* Corresponding author. Tel.: +1 915 747 5822.
E-mail addresses: vbolborici@utep.edu (V. Bolborici), dawson@ele.utoronto.ca (F.P. Dawson), mpugh@math.utoronto.ca (M.C. Pugh).

0041-624X/$ - see front matter © 2013 Elsevier B.V. All rights reserved.
http://dx.doi.org/10.1016/j.ultras.2013.10.005

and the assumed vibration modes of the stator. This yields two matrix equations: an actuator equation and a sensor equation. The stator model developed in this paper is a very good tool for the design and optimization of this type of stators for a variety of geometries and materials. In [6] the authors present a model of the stator of a traveling wave ultrasonic motor based on the first-order shear deformation laminated plate theory applied to annular subdomains of the stator. The model uses the constitutive equations of piezoelectricity, Hamilton's principle, and the Ritz Method to obtain approximate solutions for the modified Hamilton's principle. The overall accuracy of the model is comparable to that of finite element methods (FEM) and is within 4.5% as compared with experimental data.

The models presented in [5,6] are very good for simulation but can be hard to use in developing a controller for a practical application. Specifically, the models that arise from Hamilton's principle or from FEM approaches have the unknowns multiplied by either an inertia matrix or by a mass matrix, making a direct use of the model by a controller more difficult.

This paper proposes a method of modeling the stator of a piezoelectric traveling wave rotary ultrasonic motor by building upon the finite volume method (FVM) model of a unimorph plate presented in [7]. The goal of the modeling is to approximate the operating frequency of the stator of the motor; simulations of the model are compared to experimental measurements of an ultrasonic motor Shinsei USR60. These experiments show that the operating frequency of the real stator was within 1% by the simulations of the model.

In the FVM model presented here, the region of interest is divided into subregions and the unknowns are the average displacement of each subregion. Such averaged quantities are often exactly what a sensor or controller needs to work with. The FVM approach then yields a system of first-order ordinary differential equations that the average displacements satisfy. These differential equations can be interpreted directly as equivalent circuits and used by a controller.

It was shown in [8,9,7] that the finite volume method has the following strengths when it comes to modeling piezoelectric devices:

(a) The FVM ordinary differential equations can be interpreted intuitively in terms of coupled circuits that represent the piezoelectric system [8]. These circuits can then be implemented using schematic capture packages. This makes it easier to interface the FVM model of the piezoelectric system with control circuits.
(b) The flux continuity is preserved across the boundaries exactly thus allowing complex boundary conditions to be handled with more precision. Therefore, this method may be more suitable to model an ultrasonic motor because the operating principle of the motor is based on the friction mechanism that takes place at the common contact boundary between the stator and the rotor.

2. Modeling an ultrasonic motor stator

The stator of an ultrasonic motor Shinsei USR60 is studied. The stator is made of a piezoelectric ring bonded with an adhesive to a metal ring (see Fig. 1). The adhesive layer is thin compared to the metal and the piezoelectric rings. For this reason, the metal and piezoelectric rings are modeled, but the adhesive layer is not. The piezoelectric ring is divided into two semicircular sectors A and B, as shown in Fig. 2. Each sector contains eight "active regions" labeled by "+" or "−" in Fig. 2. The "+" or "−" labellings reflect the fact that the regions have opposite polarizations. This means that if a positive DC voltage is applied to both regions, the "+" regions will expand and the "−" regions will contract; seen from the side, the resulting deformation will look like that shown in Fig. 3a. All eight active regions of sector A are electrically connected by a common electrode; the supply voltage is applied simultaneously to all eight. As a result, when a positive DC voltage is applied to sector A, each of the eight active regions in sector A will deform as shown in Fig. 3a. Alternatively, when a negative DC voltage is applied to sector A, the active regions in sector A will deform as shown in Fig. 3b. Because sector A is coupled to the rest of the stator, the entire stator will deform.

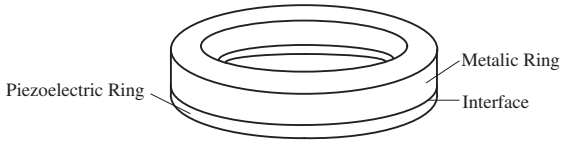

Fig. 1. Ultrasonic motor stator structure.

If an AC voltage is applied to sector A at the operating frequency, then a standing wave with nine wavelengths will form in the entire stator. Similarly, the eight active regions of sector B are also electrically connected by their own common electrode and so, if either sector A or sector B is driven with an AC voltage at the operating frequency then a standing wave forms. However, if they are driven with equal-amplitude AC voltages that are at the same operating frequency but are out of phase by 90° then a traveling wave can form, allowing the motor to operate as a two-phase motor. The 90° phase difference is determined by the length of the passive region at the top of the rotor (see Fig. 2); it is a quarter wavelength. The goal of the modeling in this article is to find a relatively simple model that will identify this operating frequency of the stator.

Each ± pair of active regions corresponds to one ninth of the total ring and, for modeling simplicity, the stator is viewed as having nine "wavelength sectors"—the extra wavelength's worth of passive material at the top and bottom of the ring shown in Fig. 2 is replaced by a wavelength sector. In this way, the full stator can be modeled as nine identical wavelength sectors, each one coupled to its flanking sectors (see Fig. 2). Fig. 4a shows a sector of width w_s. Its outer length (marked λ) is $2\pi R/9$ and its inner length is $2\pi r/9$ where R and r are the outer and inner radii, respectively. Because each wavelength sector behaves the same way, rather than

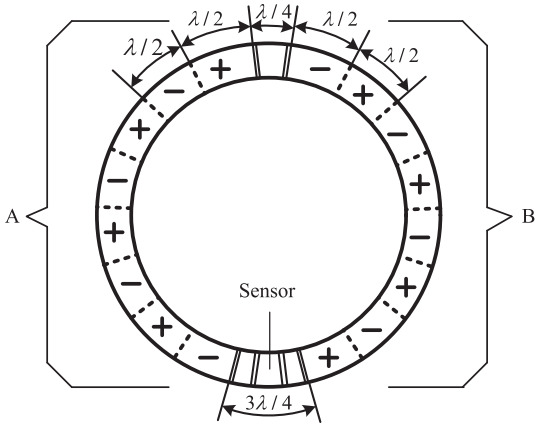

Fig. 2. The piezoelectric ring has an external diameter of 60 mm, an internal diameter of 45 mm, and a thickness of 0.5 mm. The regions A and B are composed of active regions denoted by "+" and "−". There are nine wavelengths: $9\lambda = 2\pi R$ where R is the outer radius. The regions A and B are separated by a passive region of width $\lambda/4$ at the top and a passive region of width $3\lambda/4$ at the bottom. The bottom region is used as a sensor, generating a voltage proportional to the amplitude of the traveling wave.

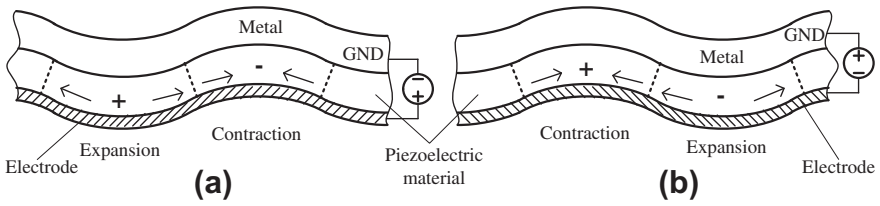

Fig. 3. Deformation modes for which the eigenfrequencies are calculated.

modeling nine wavelength sectors in a ring configuration, a single wavelength sector is studied with periodic boundary conditions.

Another modeling simplification is made by modeling the curved wavelength sector of Fig. 4 with a straightened equivalent rectangular sector, as shown in Fig. 5. Such a straightening approximation will affect the eigenmodes and the distribution of the eigenfrequencies. The eigenmodes of the wavelength sector involve Bessel functions while those of the rectangular sector are based on sin and cos. As a result, the eigenfrequencies will be different. The less curved the wavelength sector, the more valid this straightening approximation will be. The key quantities in the approximation are the angle subtended ($\lambda/(2\pi R)$) and the ratio of the sector width to the radius (w_s/R) in Fig. 4. The smaller these quantities the better the straightening approximation will be. The inner radius of the USR60 motor is only three times the width of the stator ring and there are only nine sectors and so the straightening approximation is somewhat crude. But one should not forget that there are other factors in the model that also introduce modeling errors. For example, the assumption of a constant, unidirectional electric field, as discussed in Section 3.

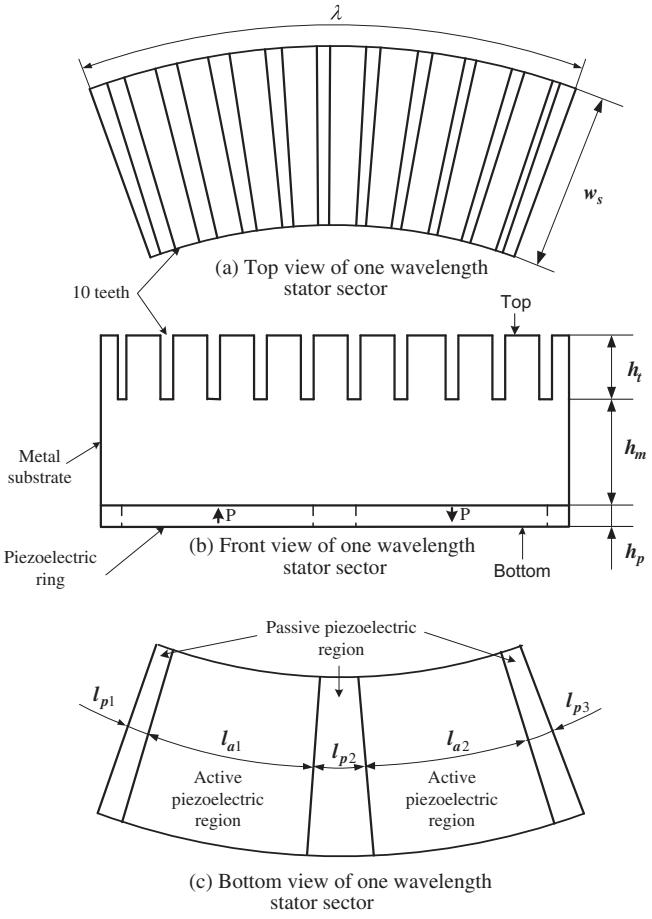

Fig. 4. A wavelength sector of the ultrasonic motor stator.

Fig. 4c shows five regions in the piezoelectric material of the one wavelength stator sector: three passive regions of average lengths l_{p1}, l_{p2}, and l_{p3}, and two active ("+" or "−") regions of average lengths l_{a1} and l_{a2}. Measurements of the Shinsei USR60 stator yield:

$$l_{p1} = l_{p3} = 0.00035 \text{ m}, \quad l_{p2} = 0.0007 \text{ m}$$
$$l_{a1} = l_{a2} = 0.00846 \text{ m}, \quad w_s = 0.0075 \text{ m}$$
$$h_p = 0.0005 \text{ m}, \quad h_m = 0.00255 \text{ m}, \quad h_t = 0.001225 \text{ m}$$

The inner and outer radii are 0.0225 m and 0.03 m respectively; the average radius is 0.02625 m. The average length of a sector is then $2\pi(.02625)/9 \approx .01832$ m. The lengths l_{p1}, l_{p2}, l_{p3}, l_{a1}, and l_{a2} were based on this length, using measurements of the angles subtended by the active and passive regions.

The rectangular sector shown in Fig. 5 is taken to scale with the wavelength sector shown in Fig. 4 with physical dimensions:

$$l_s = 0.01832 \text{ m} = l_{p1} + l_{p2} + l_{p3} + l_{a1} + l_{a2}$$
$$w_s = 0.0075 \text{ m}$$
$$h_p = 0.0005 \text{ m}$$
$$h_m = 0.00255 \text{ m}$$

The wavelength sector has ten "teeth", each of height h_t (see Fig. 4b) but the rectangular sector does not (see Fig. 5b). To determine the importance of these teeth, exploratory COMSOL simulations were performed. As expected, when the deformations are relatively small the teeth have little effect on the overall rigidity of the material—the tips of the teeth do not touch one another because of the gaps between the teeth (see [8] for the simulations). For this reason, the teeth are not included in the equivalent rectangular sector—the metal is taken to be height h_m rather than $h_m + h_t$. Although the teeth are not included in the geometry, their mass is included. This is done by using a larger, "effective" density so that the metal plate of height h_m of Fig. 5 has the same mass as a copper plate of height $h_m + h_t$. The mass density for copper is 8700 kg/m^3 yielding an equivalent mass density of 12,881 kg/m^3 for the equivalent rectangular sector.

As shown in Fig. 4, the piezoelectric part of the wavelength sector has five subregions: two active and three passive. To determine the stress in the material from the strain and the electric field, a stiffness (or elasticity) matrix and an electromechanical coupling matrix are used (see Eq. (4)). These matrices are determined by material properties, including the polarization. All five subregions have the same stiffness matrix. The active regions have polarizations that differ by 180° and so their electromechanical coupling matrices are the same. The passive regions in Fig. 4 are not polarized; their electromechanical coupling matrices are different from the active regions' matrices, resulting in internal boundaries. Also, the passive region at the top in Fig. 2 and the passive regions flanking the sensor at the bottom are not polarized; the passive region containing the sensor is. In both Figs. 2 and 4c, these internal boundaries are represented by the segments that connect the inner radius to the outer radius.

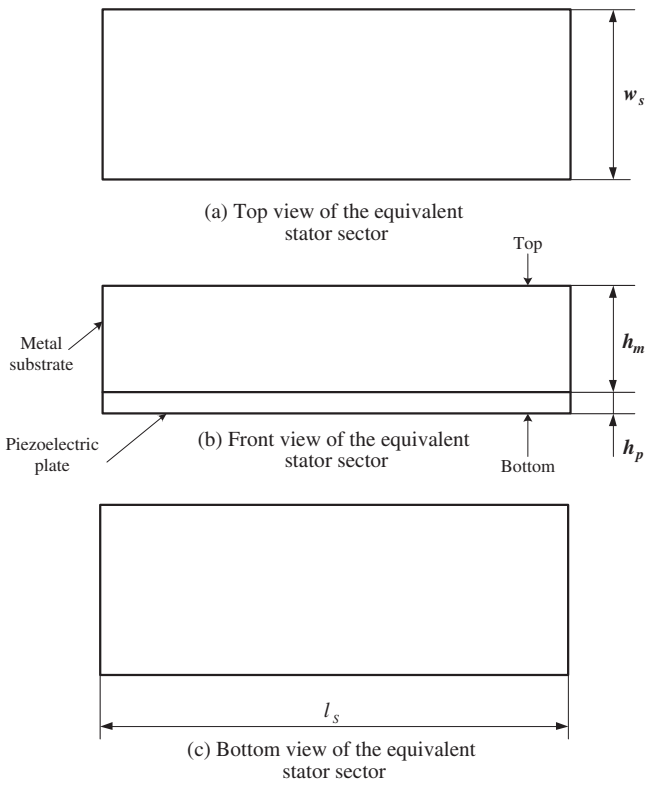

Fig. 5. The equivalent rectangular sector for a wavelength sector of the ultrasonic motor stator.

The modeling goal is to find the operating frequency of the stator: the frequency at which each wavelength sector deforms as shown in Fig. 3. This frequency corresponds to a particular eigenfrequency of the wavelength sector shown in Fig. 4. These eigenfrequencies do not depend on the imposed electric field and so are not affected by the values of the electromechanical matrices. For this reason, a simplifying assumption is made in the modeling: the entire stator is approximated by a single polarized piezoelectric material, with the same polarization. As a result there are no internal boundaries and, for the purposes of an eigenfrequency study, the entire straightened region shown in Fig. 5 is assumed to have the same polarization.

In [7], the authors present an FVM model for a unimorph piezoelectric plate. The model presented here builds upon that model with the following modifications: the curved sector of the stator is approximated by a straightened one, periodic boundary conditions are applied at the ends, and the teeth of the stator are neglected and a larger effective density is used to reflect the lost mass.

3. The partial differential equations model

The finite volume model of the stator is obtained by discretizing a partial differential equations model of the stator. The partial differential equation model of the stator describes the local behavior of the piezoelectric material and metal. It is obtained by combining Newton's second law for local behavior in a bulk material with the constitutive equation of piezoelectricity, the boundary conditions, and Maxwell's equation for electrostatics without sources or sinks of free charge.

The dynamics of the piezoelectric material are determined from Newton's second law [10]

$$\rho \frac{\partial^2 \mathbf{u}}{\partial t^2} = \rho \mathbf{u}_{tt} = \nabla \cdot \mathbf{T} \tag{1}$$

the absence of sources or sinks of charge

$$\nabla \cdot (\mathbf{eS} + \boldsymbol{\varepsilon}^{\mathbf{S}} \mathbf{E}) = 0 \tag{2}$$

and appropriate boundary conditions. Above, ρ is the mass density of the piezoelectric material and

$$\mathbf{u}(x,y,z,t) = \begin{pmatrix} u(x,y,z,t) \\ v(x,y,z,t) \\ w(x,y,z,t) \end{pmatrix} \tag{3}$$

where u, v, and w are the local displacements from rest in the x, y, and z directions respectively. $\mathbf{T}(x,y,z,t)$ is the stress; $\mathbf{S}(x,y,z,t)$ is the strain; $\mathbf{E}(x,y,z,t)$ is the electric field; the electromechanical coupling matrix is $\mathbf{e}$ and $\boldsymbol{\varepsilon}^{\mathbf{S}}$ is the dielectric matrix, evaluated at constant strain. The actuator equation

$$\mathbf{T} = \mathbf{c}^{\mathbf{E}} \mathbf{S} - \mathbf{e}^t \mathbf{E} \tag{4}$$

gives the stress as a function of the strain and the electric field, at each point in the material, at each moment in time. The superscript t in (4) denotes the transpose, $\mathbf{c}^{\mathbf{E}}$ is the stiffness or elasticity matrix.

There are three types of boundary conditions for the equivalent rectangular sector of Fig. 5. At the ends, where one sector meets the flanking sectors, the displacements at the left end are assumed to equal the displacements at the right end. This corresponds to periodic boundary conditions for the model of a single sector. At the external, free boundaries (at the top, bottom, front and back in Fig. 5) there are zero stress boundary conditions. At the internal boundary, where the metal and piezoelectric meet, the limiting value of the displacements as taken from within the metal are assumed to equal the limiting value of the displacements as taken from within the piezoelectric material.

The final modeling assumption is that the piezoelectric material is assumed to be thin in the z direction (see Fig. 5b) and the electric field $\mathbf{E}$ is assumed to be constant and unidirectional:

$$\mathbf{E}(x,y,z,t) = (0,0,E_3)^t. \tag{5}$$

In this case, Eqs. (1) and (4) determine $\mathbf{u}$.

Eq. (1) is valid for both piezoelectric material and metal. In this equation ρ is the mass density of the piezoelectric material, when the equation describes the local behavior of the piezoelectric material, and is the mass density of the metal, when the equation describes the local behavior of the metal. The actuator Eq. (4) can also be used for both piezoelectric material and metal. For piezoelectric material, this equation contains both terms on the right hand side. $\mathbf{c}^{\mathbf{E}}$ is the stiffness matrix and $\mathbf{e}$ is the electromechanical coupling matrix of the piezoelectric material. For metal, Eq. (4) loses the second term on the right hand side as the metal does not have piezoelectric properties ($\mathbf{e} = 0$). In this equation $\mathbf{c}^{\mathbf{E}}$ is the stiffness matrix of metal.

4. Numerical results

In [9], a thin piezoelectric plate was studied using the finite volume method (FVM) to discretize Eqs. (1) and (4). When using the FVM to discretize the partial differential equations, one starts by dividing the domain into "control volumes" and averaging the partial differential equations over each one. This yields a system of ordinary differential equations for each volume. The structure of the system of ordinary differential equations is different for *internal volumes* (all six faces are internal to the metal or to the piezoelectric), *face volumes* (one face is at an external boundary or at the metal/piezo interface), *edge volumes* (two faces are at an external boundary or at the metal/piezo interface), and *corner volumes* (three faces are at an external boundary or at the metal/piezo interface). In [9], the ordinary differential equations for internal

volumes (37)–(39) (also shown as Eqs. (B.1), (B.2) and (B.3) in Appendix B) are presented.

At face volumes that have faces at external boundaries, the ordinary differential equations (37)–(39) of [9] (Eqs. (B.1), (B.2) and (B.3) in Appendix B) are supplemented by boundary equations which reflect the boundary conditions. The equivalent rectangular sector of Fig. 5 has four free faces at which there are zero-stress boundary conditions; here, the boundary equations (165)–(176) of [9] (Eqs. (B.10)–(B.20) and (B.21) in Appendix B) are used with stresses $t_i = 0$ for $i = 1, \ldots, 6$. In addition, there are two "external" boundaries that are identified with one another to reflect the presence of identical equivalent rectangular sectors on each side. To do this, boundary equations. (49)–(51) and (162)–(164) of [9] (Eqs. (B.4)–(B.8) and (B.9) in Appendix B) are replaced by periodic conditions

$$u_W = u_E, \quad v_W = v_E, \quad w_W = w_E. \tag{6}$$

The first equation means that the x-displacement at the left face of Fig. 5b, u_W, equals the x-displacement at the right face of Fig. 5b, u_E. The second and third equations are interpreted similarly.

In [7], the FVM approach was extended to model a unimorph structure: a metal plate bonded to a piezoelectric plate. Such a structure has an internal boundary where the metal and piezoelectric material meet. The control volumes were chosen to flank this internal boundary: one control volume would be fully in the metal with a face in the internal boundary and on the other side of the internal boundary would be a second control volume that is fully within the piezoelectric material. The boundary conditions at this internal boundary then appear in the FVM model via boundary equations; for example, see (7)–(9) in [7] (Eqs. (B.44)–(B.49) and (B.50) in Appendix B). These boundary equations are used at the internal boundary of the equivalent rectangular sector.

4.1. The system of equations

The system of equations for the equivalent rectangular sector shown in Fig. 5 consists of the ordinary differential Eqs. (37)-(39) (Eqs. (B.1), (B.2) and (B.3) in Appendix B) with boundary equations (165)-(200) from [9] (Eqs. (B.10)–(B.42) and (B.43) in Appendix B) (with $t_i = 0$ for $i = 1 \ldots, 6$), the boundary equations (7)-(9) from [7] (Eqs. (B.44)–(B.49) and (B.50) in Appendix B), and the boundary Eq. (6). This results in a system of ordinary differential equations of the form

$$\frac{d}{dt}\mathbf{X} = \mathbf{A_1}\,\mathbf{X} + \mathbf{B_1} \tag{7}$$

where $\mathbf{A_1}$ is the system matrix, vector $\mathbf{B_1}$ includes the forces due the electric field and the boundary conditions and the vector $\mathbf{X}$ contains the averaged displacements and the averaged velocities for each finite volume. The system of Eq. (7) can then be solved using a program such as Matlab (The MathWorks Inc., Natick, MA).

4.2. Eigenfrequency analysis

An eigenfrequency analysis of the FVM model (7) is performed. This consists of calculating the system matrix A_1 and finding its eigenvectors and eigenvalues. For a given eigenvector the displacement is reconstructed. Deformations for which half of the control volumes move up and half move down (e.g. Fig. 3) are identified[1] and the one with the lowest eigenvalue is used as a diagnostic; it corresponds to the fundamental frequency for that particular discretization.

[1] Specifically, deformations for which there are two points with zero displacement are identified.

Table 1
The fundamental eigenfrequency for the equivalent rectangular sector, calculated with the proposed FVM model for different numbers of control volumes, the corresponding degrees of freedom (DoF), the deviation from the best available approximation of the eigenfrequency (39,119 Hz), and the simulation time.

Volumes	DoF	Freq. (Hz)	Approx. rel. error (%)	Simulation time (s)
12	72	52,326	33.76	1.7
36	216	45,661	16.72	8.5
72	432	42,919	9.71	22
120	720	41,748	6.72	53
180	1080	41,084	4.93	105
252	1512	40,709	4.06	209
500	3000	40,565	3.70	635
720	4320	40,391	3.25	1304
1008	6048	40,289	2.99	2449
1260	7560	40,238	2.86	3629
1536	9216	40,204	2.77	5547
1836	11,016	40,178	2.71	7284
2508	15,048	40,138	2.60	13,865
3240	19,440	40,080	2.46	17,256
12,400	74,400	39,626	1.30	45,537
25,920	155,520	39,446	0.84	216,154

Table 1 presents this fundamental frequency for different discretizations. Table 2 presents the analogous results found using COMSOL's FEM discretization of the partial differential Eqs. (1), (2), and (4) for the same equivalent rectangular sector (see Fig. 5). Both finite volume Matlab and finite element COMSOL simulations have been performed on a Supermicro Superserver computer with two Intel Xeon E5645 2.4 GHz processors and 192 GB RAM. In comparing the runtimes for the FEM and FVM discretizations, one must bear in mind that COMSOL is an optimized industrial product in which the implementation of the modeling equations has been optimized.

COMSOL is computing the electric field in addition to the displacements while the FVM model is taking the electric field as an imposed constant (see (5)) and so the two models will converge to slightly different limits as the discretizations get finer and finer. For the purposes of computing an (approximate) relative error for the FVM model, the eigenfrequency provided by the best–resolved COMSOL run (39,119 Hz) is taken as the "true" value. The small relative error of the FVM model (see Table 1) shows that the uniform, unidirectional assumption on $\mathbf{E}$ (see (5)) was not an extreme one.

5. Experimental results

To validate the numerical results of Section 4, experiments have been conducted with a stator of an ultrasonic motor USR60, shown in Fig. 6, using the test setup shown in Fig. 7. The rotor has been removed from the motor and the brake decoupled, allowing the stator to be studied in isolation. A motor driver supplies voltages to the semicircular sectors A and B of the stator; the response is measured by the built-in sensor located in the stator (see Fig. 2). Not having access to a laser vibrometer, the deflections of the stator have not been measured.

Three different tests have been performed to measure the frequency response of the stator. In the first test, sector A was driven with an AC voltage; sector B was passive. This driving resulted in a standing wave response of the stator. In the second test, sector B was driven while sector A was passive, again resulting in a standing wave. In the third test, both sectors A and B were driven at the same frequency. However, they are driven with a 90° phase shift, resulting in a traveling wave response.

The frequency of the driving voltage was swept between 20 kHz and 60 kHz. For each driving frequency, the sensor produces a voltage which is then rectified and filtered by a circuit built into the motor by the manufacturer. The resultant peak voltage is then

Table 2
The fundamental eigenfrequency for the equivalent rectangular sector, simulated in COMSOL for different numbers of elements in the mesh, the corresponding degrees of freedom (DoF), the deviation from the best approximation of the available eigenfrequency (39,119 Hz), and the simulation time.

Number of mesh elements	DoF	Freq. (Hz)	Rel. error (%)	Simulation time (s)
88	767	43,592	11.43	3
143	1075	42,575	8.83	4
378	2658	40,557	3.68	5
906	5836	39,883	1.95	8
1646	9933	39,635	1.32	13
2827	16,135	39,498	0.97	21
4950	25,067	39,423	0.78	32
8146	41,838	39,346	0.58	56
24,970	115,525	39,256	0.35	191
50,044	226,967	39,222	0.26	454
93,897	417,719	39,166	0.12	938
133,065	584,797	39,149	0.08	1559
220,090	954,811	39,132	0.03	2958
327,391	1,404,816	39,119		5133

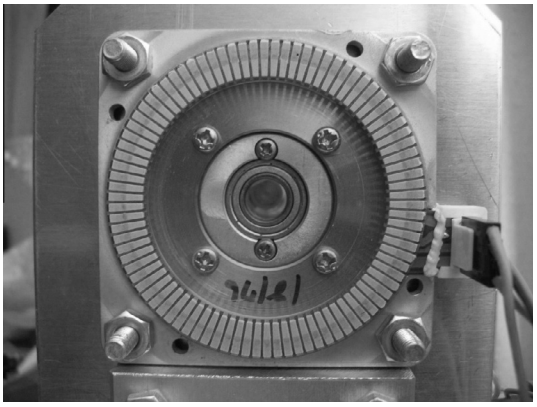

Fig. 6. The stator of a piezoelectric traveling wave rotary ultrasonic motor USR60. In order to measure the resonance frequencies of the stator in isolation, the rotor of the motor has been removed.

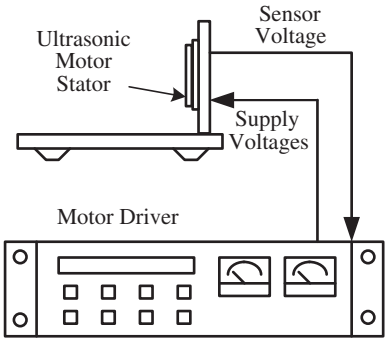

Fig. 7. The test setup contains a motor driver that can supply the stator with sinusoidal voltages at various frequencies, amplitudes, and phases. The piezoelectric motor is mounted on a platform and is coupled to a hysteresis brake not shown here. In order to measure the resonance frequencies of the stator in isolation, the brake has been decoupled and the rotor has been removed.

relayed to the motor driver (see Fig. 7). In Fig. 8, peak voltage is plotted as a function of driving frequency for each of the three tests. The larger the peak voltage, the larger amplitude of the wave in the rotor. Resonance frequencies correspond to peaks in Fig. 8. All three tests yield similar results; this is expected because the phase-A and phase-B sectors have the same dimensions (see Fig. 2).

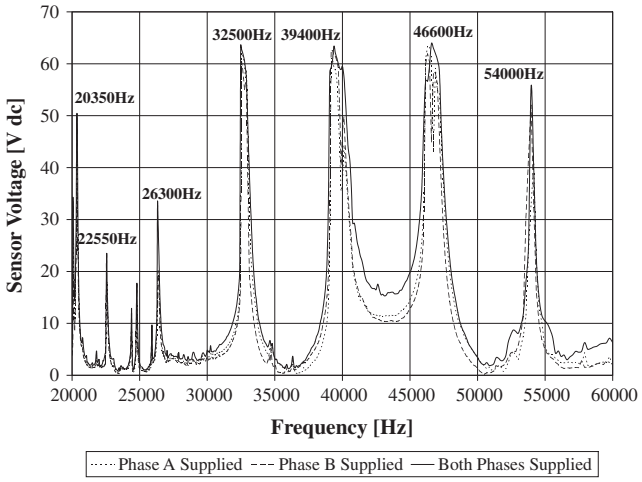

Fig. 8. The frequency response of the stator of the ultrasonic motor USR60, shown in Fig. 6. These plots represent the peak voltage of the motor's sensor versus the frequency of the supply voltages.

Table 3
The best simulated approximation of the available eigenfrequency (39,119 Hz), the experimental results for eigenfrequency for a piezoelectric motor Shinsei USR60, and the relative errors.

Method	Eigenfrequency (Hz)	Rel. error (%)
Theoretical FEM	39,119	−0.71
Theoretical FVM	39,446	0.11
Experimental	39,400	

Of the peak frequencies shown in Fig. 8, the manufacturer has selected the frequency of 39.4 kHz as the operating frequency of the stator. It corresponds to the frequency at which each of the eight wavelength sectors (see Fig. 4) has a deformation like that shown in Fig. 3. Repeating the tests with the rotor mounted on top of the stator [8], this operating frequency increases to 41–42 kHz. This is because the pressure applied by the rotor on the stator increases the stator's rigidity.

Table 3 compares the operating frequency found experimentally to the fundamental frequency found using the FVM model and the FEM model. Although a variety of approximations went into both models, the experimental results show that they are not extreme—the simulation results are within 1% of the experimental measurement.

6. Conclusions

This paper presents a method to determine the operating frequency of the stator of a USR60 piezoelectric motor, by modeling the stator with the finite volume method. Simulation results using the proposed model, and also using finite element commercial software, are presented together with experimental results. The finite element simulations compute the deformation and electric field simultaneously. The finite volume simulations assume the electric field to be uniform and unidirectional and compute the resulting deformation. The small relative error between the finite volume model and the finite element one shows that the uniform, unidirectional assumption on **E** is not an extreme one. The fundamental frequencies found by the finite element and finite volume models are within 1% of the experimental measurements of the operating frequency.

Using a numerical model to determine the operating frequency of the stator is useful in the design process of a new motor when

one wants to study various possible designs before the motor is built. This will save the designer time and money and will help with the optimization of the motor. Another potential advantage of the finite volume model presented here is that the finite volume method handles surface forces easily. This would allow the model to be easily integrated with a contact model and a rotor model. This would then allow one to determine in real time the operating frequency of the motor, which also depends on the contact between the rotor and the stator, and control the motor using an adaptive control technique by supplying the motor with voltages at frequencies close to the operating frequency. Last but not least, the finite volume model yields ordinary differential equations that can be interpreted intuitively in terms of coupled circuits that represent the stator's dynamics. These circuits can then be implemented using schematic capture packages. This makes it easier to interface the finite volume model of the stator with control circuits.

Appendix A. Material properties

The simulations were done for the piezoelectric material PZT-5H. This is not the piezoelectric material found in the Shinsei USR60 motor. The PZT-5H material was chosen as a good fit for the confidential data that the Shinsei corporation provided.

A.1. Piezoelectric material PZT-5H [11]

Mass density $\rho = 7500\ \text{kg/m}^3$

The entries of the dielectric matrix $\boldsymbol{\varepsilon}^{\mathbf{S}}$ are $\varepsilon_{11} = \varepsilon_{22} = 1704.40$ and $\varepsilon_{33} = 1433.61$ F/m.

The entries of the stiffness matrix $\mathbf{c}^{\mathbf{E}}$ are $c_{11} = c_{22} = 1.272 \times 10^{11}\ \text{N/m}^2$, $c_{33} = 1.174 \times 10^{11}\ \text{N/m}^2$, $c_{44} = 2.298 \times 10^{10}\ \text{N/m}^2$, $c_{55} = 2.298 \times 10^{10}\ \text{N/m}^2$, $c_{66} = 2.347 \times 10^{10}\ \text{N/m}^2$, $c_{12} = c_{21} = 8.021 \times 10^{10}\ \text{N/m}^2$, and $c_{13} = c_{31} = c_{23} = c_{32} = 8.467 \times 10^{10}\ \text{N/m}^2$.

The entries of the electromechanical coupling matrix $\mathbf{e}$ are: $e_{31} = e_{32} = -6.622\ \text{N/(Vm)}$, $e_{33} = 23.24\ \text{N/(Vm)}$, and $e_{15} = e_{24} = 17.03\ \text{N/(Vm)}$.

The coefficients have a tolerance of ±20%:
http://www.sinocera.net/en/piezo_material.asp

A.2. Copper [11]

Mass density is $\rho = 8700\ \text{kg/m}^3$, Young modulus $E = 110 \times 10^9\ \text{N/m}^2$, and Poisson ratio $\nu = 0.35$. Hence $c_{11} = c_{22} = c_{33} = c_{12} = c_{13} = c_{21} = c_{23} = c_{31} = c_{32} = \nu E/(1-\nu^2)$ and $c_{44} = c_{55} = c_{66} = E/(2+2\nu)$.

Appendix B. Finite volume equations

The following equations, their coefficients, and figures that show the distances used in the equations are the FVM discretization presented in [9,7]. They are provided in this appendix in order to make this a stand-alone paper. Eqs. (B.1), (B.2) and (B.3) model the dynamics of the (average) displacement of a volume: $\mathbf{u}_p = \langle u_p, v_p, w_p \rangle$.

$$\begin{aligned}\frac{d^2u_P}{dt^2} = {} & -P_1u_P + \varepsilon_1u_E + W_1u_W + N_1u_N + S_1u_S + F_1u_F + R_1u_R \\ & + B_{11}(v_N - v_S) + B_{12}(v_{NE} - v_{SE}) - B_{13}(v_{NW} - v_{SW}) \\ & + B_{14}(v_E - v_W) + B_{15}(v_{NE} - v_{NW}) - B_{16}(v_{SE} - v_{SW}) \\ & + B_{17}(w_F - w_R) + B_{18}(w_{FE} - w_{RE}) - B_{19}(w_{FW} - w_{RW}) \\ & + B_{110}(w_E - w_W) + B_{111}(w_{FE} - w_{FW}) - B_{112}(w_{RE} - w_{RW})\end{aligned} \tag{B.1}$$

$$\begin{aligned}\frac{d^2v_P}{dt^2} = {} & -P_2v_P + \varepsilon_2v_E + W_2v_W + N_2v_N + S_2v_S + F_2v_F \\ & + R_2v_R + B_{21}(u_N - u_S) + B_{22}(u_{NE} - u_{SE}) - B_{23}(u_{NW} \\ & - u_{SW}) + B_{24}(u_E - u_W) + B_{25}(u_{NE} - u_{NW}) - B_{26}(u_{SE} \\ & - u_{SW}) + B_{27}(w_F - w_R) + B_{28}(w_{FN} - w_{RN}) - B_{29}(w_{FS} \\ & - w_{RS}) + B_{210}(w_N - w_S) + B_{211}(w_{FN} - w_{FS}) \\ & - B_{212}(w_{RN} - w_{RS})\end{aligned} \tag{B.2}$$

$$\begin{aligned}\frac{d^2w_P}{dt^2} = {} & -P_3w_P + \varepsilon_3w_E + W_3w_W + N_3w_N + S_3w_S + F_3w_F \\ & + R_3w_R + B_{31}(u_F - u_R) + B_{32}(u_{FE} - u_{RE}) - B_{33}(u_{FW} - u_{RW}) \\ & + B_{34}(u_E - u_W) + B_{35}(u_{FE} - u_{FW}) - B_{36}(u_{RE} - u_{RW}) \\ & + B_{37}(v_F - v_R) + B_{38}(v_{FN} - v_{RN}) - B_{39}(v_{FS} - v_{RS}) \\ & + B_{310}(v_N - v_S) + B_{311}(v_{FN} - v_{FS}) - B_{312}(v_{RN} - v_{RS})\end{aligned} \tag{B.3}$$

The quantities u_E, v_E, etc. refer to displacements at the faces of a volume; see Figs. B.9–B.14 for the notation. These quantities are approximated using displacements of neighboring volumes and using boundary conditions; see Eqs. (B.4)–(B.49) and (B.50) and Figs.B.15–B.22. The coefficients are given in Eqs. (B.51–B.137).

$$u_E = u_P - A_{E1}(v_{NE} - v_{SE}) - A_{E2}(w_{FE} - w_{RE}) + A_{E3}E_3 + \frac{\delta_{XE}}{c_{11}}t_1 \tag{B.4}$$

$$v_E = v_P - A_{E4}(u_{NE} - u_{SE}) + \frac{\delta_{XE}}{c_{66}}t_6 \tag{B.5}$$

$$w_E = w_P - A_{E5}(u_{FE} - u_{RE}) + \frac{\delta_{XE}}{c_{55}}t_5 \tag{B.6}$$

$$u_W = u_P + A_{W1}(v_{NW} - v_{SW}) + A_{W2}(w_{FW} - w_{RW}) - A_{W3}E_3 + \frac{\delta_{XW}}{c_{11}}t_1 \tag{B.7}$$

$$v_W = v_P + A_{W4}(u_{NW} - u_{SW}) + \frac{\delta_{XW}}{c_{66}}t_6 \tag{B.8}$$

$$w_W = w_P + A_{W5}(u_{FW} - u_{RW}) + \frac{\delta_{XW}}{c_{55}}t_5 \tag{B.9}$$

$$u_N = u_P - A_{N1}(v_{NE} - v_{NW}) + \frac{\delta_{YN}}{c_{66}}t_6 \tag{B.10}$$

$$v_N = v_P - A_{N2}(u_{NE} - u_{NW}) - A_{N3}(w_{FN} - w_{RN}) + A_{N4}E_3 + \frac{\delta_{YN}}{c_{22}}t_2 \tag{B.11}$$

$$w_N = w_P - A_{N5}(v_{FN} - v_{RN}) + \frac{\delta_{YN}}{c_{44}}t_4 \tag{B.12}$$

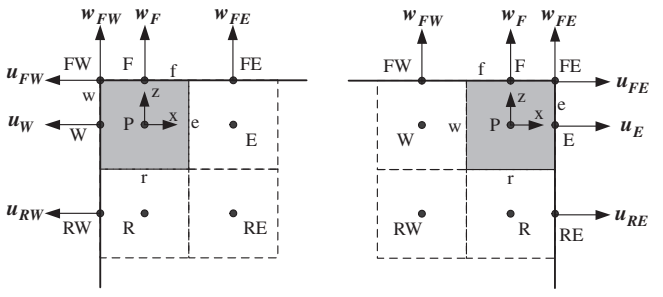

Fig. B.9. Control volumes and boundary displacements placed at the Front-West or Front-East boundaries.

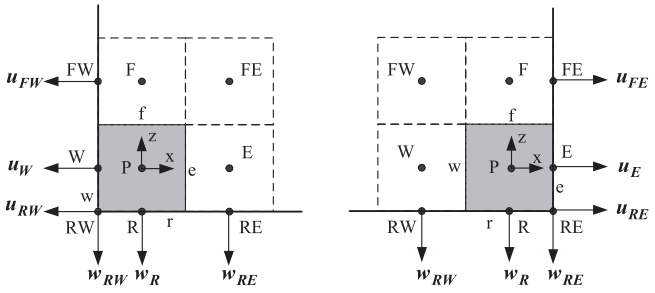

Fig. B.10. Control volumes and boundary displacements placed at the Rear-West or Rear-East boundaries.

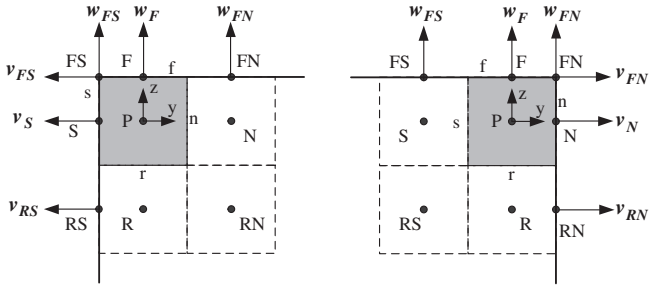

Fig. B.11. Control volumes and boundary displacements placed at the Front-South or Front-North boundaries.

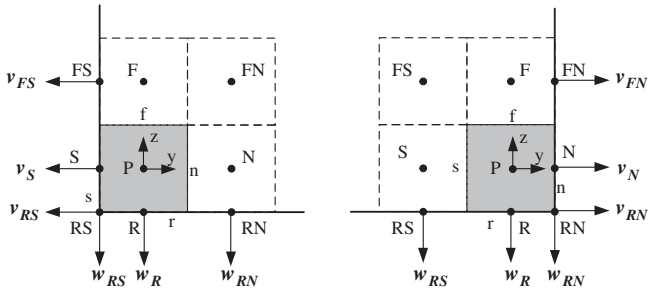

Fig. B.12. Control volumes and boundary displacements placed at the Rear-South or Rear-North boundaries.

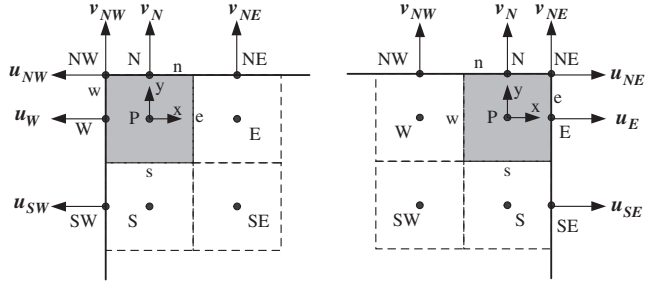

Fig. B.13. Control volumes and boundary displacements placed at the North-West or North-East boundaries.

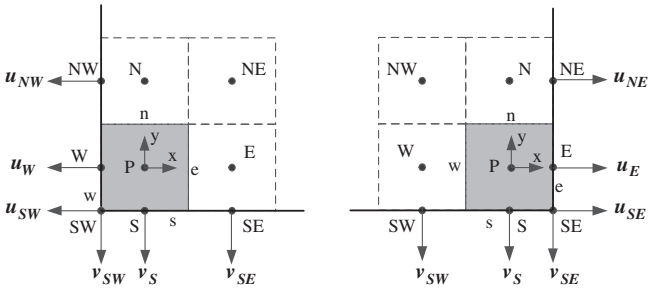

Fig. B.14. Control volumes and boundary displacements placed at the South-West or South-East boundaries.

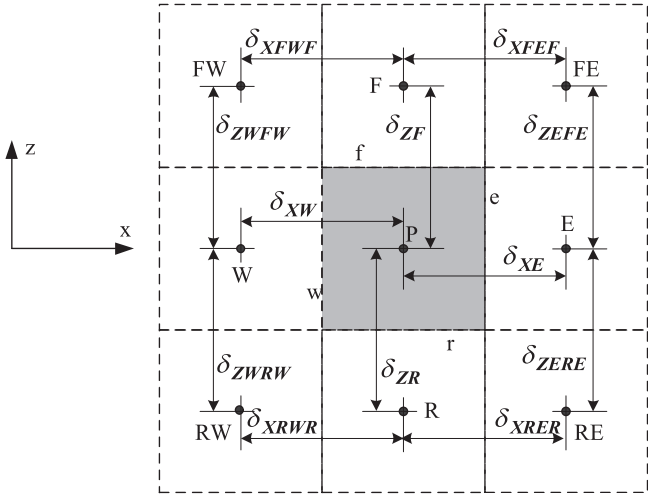

Fig. B.15. An *xz* slice through the center of the interior control volume.

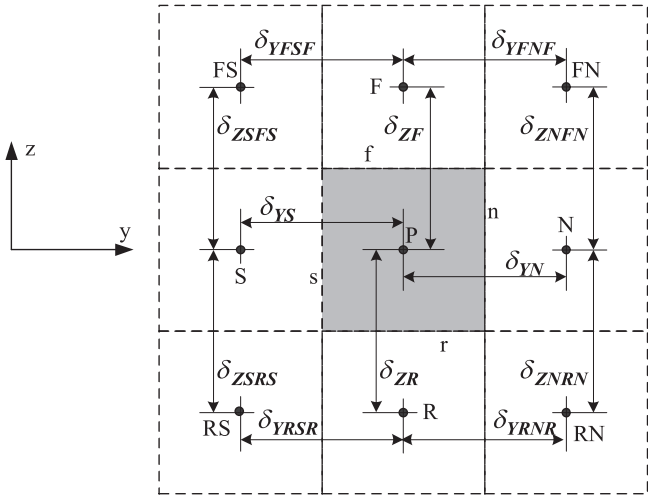

Fig. B.16. An *yz* slice through the center of the interior control volume.

$$u_S = u_P + A_{S1}(v_{SE} - v_{SW}) + \frac{\delta_{YS}}{c_{66}} t_6 \tag{B.13}$$

$$v_S = v_P + A_{S2}(u_{SE} - u_{SW}) + A_{S3}(w_{FS} - w_{RS}) - A_{S4}E_3 + \frac{\delta_{YS}}{c_{22}} t_2 \tag{B.14}$$

$$w_S = w_P + A_{S5}(v_{FS} - v_{RS}) + \frac{\delta_{YS}}{c_{44}} t_4 \tag{B.15}$$

$$u_F = u_P - A_{F1}(w_{FE} - w_{FW}) + \frac{\delta_{ZF}}{c_{55}} t_5 \tag{B.16}$$

$$v_F = v_P - A_{F2}(w_{FN} - w_{FS}) + \frac{\delta_{ZF}}{c_{44}} t_4 \tag{B.17}$$

$$w_F = w_P - A_{F3}(u_{FE} - u_{FW}) - A_{F4}(v_{FN} - v_{FS}) + A_{F5}E_3 + \frac{\delta_{ZF}}{c_{33}} t_3 \tag{B.18}$$

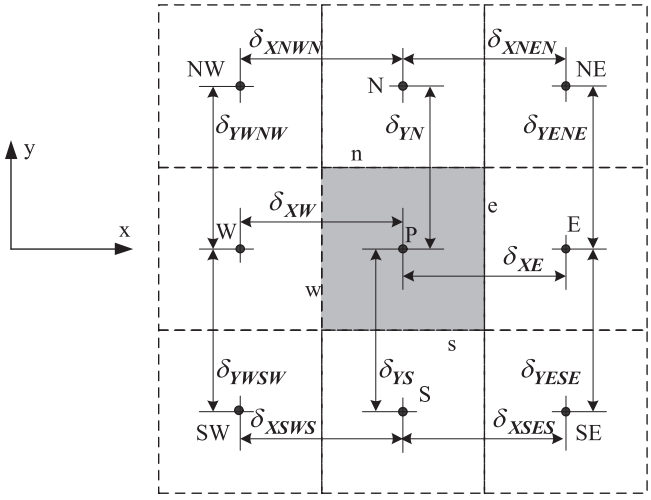

Fig. B.17. An *xy* slice through the center of the interior control volume.

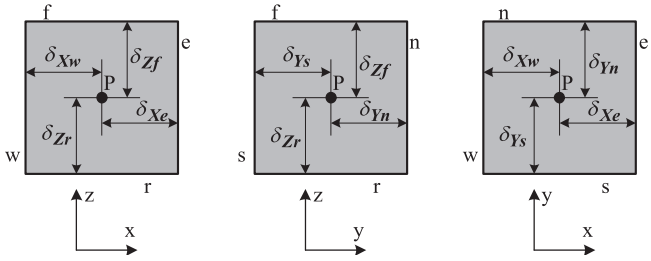

Fig. B.18. Internal distances in the control volume of interest.

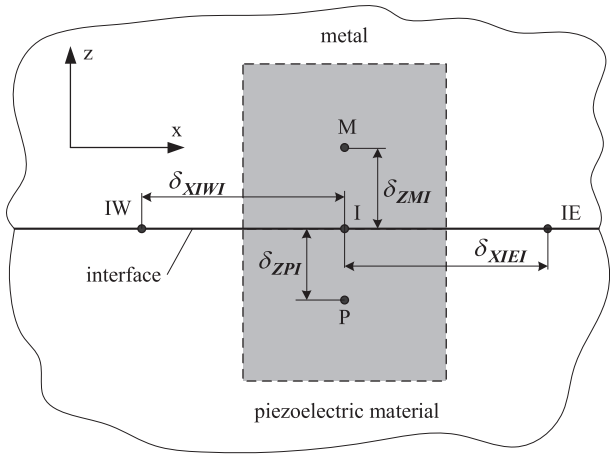

Fig. B.19. The metal-piezoelectric material interface in the *xz* plane.

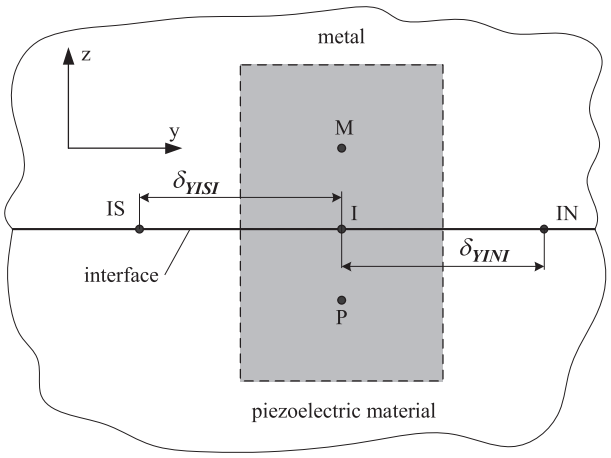

Fig. B.20. The metal-piezoelectric material interface in the *yz* plane.

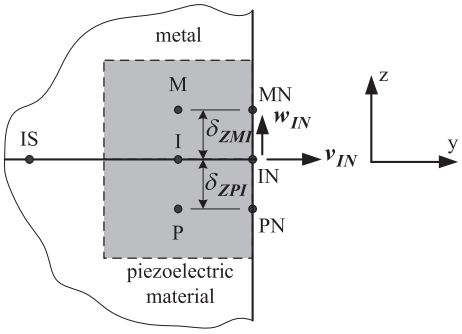

Fig. B.21. The metal-piezoelectric material interface in the *yz* plane at the North boundary.

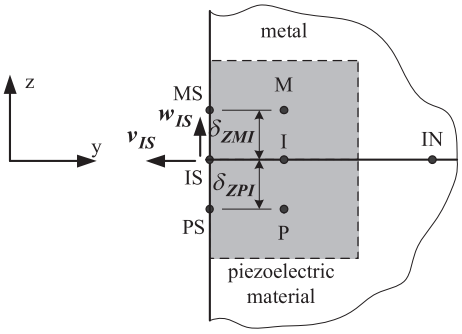

Fig. B.22. The metal-piezoelectric material interface in the *yz* plane at the South boundary.

$$u_R = u_P + A_{R1}(w_{RE} - w_{RW}) + \frac{\delta_{ZR}}{c_{55}} t_5 \tag{B.19}$$

$$v_R = v_P + A_{R2}(w_{RN} - w_{RS}) + \frac{\delta_{ZR}}{c_{44}} t_4 \tag{B.20}$$

$$w_R = w_P + A_{R3}(u_{RE} - u_{RW}) + A_{R4}(v_{RN} - v_{RS}) - A_{R5}E_3 + \frac{\delta_{ZR}}{c_{33}} t_3 \tag{B.21}$$

$$u_{FE} = u_E + \frac{\delta_{ZEFE}}{\delta_{ZERE}}(u_E - u_{RE}) \tag{B.22}$$

$$w_{FE} = w_F + \frac{\delta_{XFEF}}{\delta_{XFWF}}(w_F - w_{FW}) \tag{B.23}$$

$$u_{FW} = u_W + \frac{\delta_{ZWFW}}{\delta_{ZWRW}}(u_W - u_{RW}) \tag{B.24}$$

$$w_{FW} = w_F + \frac{\delta_{XFWF}}{\delta_{XFEF}}(w_F - w_{FE}) \tag{B.25}$$

$$u_{RW} = u_W + \frac{\delta_{ZWRW}}{\delta_{ZWFW}}(u_W - u_{FW}) \tag{B.26}$$

$$w_{RW} = w_R + \frac{\delta_{XRWR}}{\delta_{XRER}}(w_R - w_{RE}) \tag{B.27}$$

$$u_{RE} = u_E + \frac{\delta_{ZERE}}{\delta_{ZEFE}}(u_E - u_{FE}) \tag{B.28}$$

$$w_{RE} = w_R + \frac{\delta_{XRER}}{\delta_{XRWR}}(w_R - w_{RW}) \tag{B.29}$$

$$v_{FS} = v_S + \frac{\delta_{ZSFS}}{\delta_{ZSRS}}(v_S - v_{RS}) \tag{B.30}$$

$$w_{FS} = w_F + \frac{\delta_{YFSF}}{\delta_{YFNF}}(w_F - w_{FN}) \tag{B.31}$$

$$v_{FN} = v_N + \frac{\delta_{ZNFN}}{\delta_{ZNRN}}(v_N - v_{RN}) \tag{B.32}$$

$$w_{FN} = w_F + \frac{\delta_{YFNF}}{\delta_{YFSF}}(w_F - w_{FS}) \tag{B.33}$$

$$v_{RS} = v_S + \frac{\delta_{ZSRS}}{\delta_{ZSFS}}(v_S - v_{FS}) \tag{B.34}$$

$$w_{RS} = w_R + \frac{\delta_{YRSR}}{\delta_{YRNR}}(w_R - w_{RN}) \tag{B.35}$$

$$u_{NW} = u_W + \frac{\delta_{YWNW}}{\delta_{YWSW}}(u_W - u_{SW}) \tag{B.36}$$

$$v_{NW} = v_N + \frac{\delta_{XNWN}}{\delta_{XNEN}}(v_N - v_{NE}) \tag{B.37}$$

$$u_{NE} = u_E + \frac{\delta_{YENE}}{\delta_{YESE}}(u_E - u_{SE}) \tag{B.38}$$

$$v_{NE} = v_N + \frac{\delta_{XNEN}}{\delta_{XNWN}}(v_N - v_{NW}) \tag{B.39}$$

$$u_{SW} = u_W + \frac{\delta_{YWSW}}{\delta_{YWNW}}(u_W - u_{NW}) \tag{B.40}$$

$$v_{SW} = v_S + \frac{\delta_{XSWS}}{\delta_{XSES}}(v_S - v_{SE}) \tag{B.41}$$

$$u_{SE} = u_E + \frac{\delta_{YESE}}{\delta_{YENE}}(u_E - u_{NE}) \tag{B.42}$$

$$v_{SE} = v_S + \frac{\delta_{XSES}}{\delta_{XSWS}}(v_S - v_{SW}) \tag{B.43}$$

$$\begin{aligned} u_I = {} & \left(u_P \frac{c_{55p}}{\delta_{ZPI}} + u_M \frac{c_{55m}}{\delta_{ZMI}}\right) \Big/ \left(\frac{c_{55p}}{\delta_{ZPI}} + \frac{c_{55m}}{\delta_{ZMI}}\right) \\ & - (w_{IE} - w_{IW}) \frac{c_{55p} - c_{55m}}{\delta_{XIEI} + \delta_{XIWI}} \Big/ \left(\frac{c_{55p}}{\delta_{ZPI}} + \frac{c_{55m}}{\delta_{ZMI}}\right) \end{aligned} \tag{B.44}$$

$$\begin{aligned} v_I = {} & \left(v_P \frac{c_{44p}}{\delta_{ZPI}} + v_M \frac{c_{44m}}{\delta_{ZMI}}\right) \Big/ \left(\frac{c_{44p}}{\delta_{ZPI}} + \frac{c_{44m}}{\delta_{ZMI}}\right) \\ & - (w_{IN} - w_{IS}) \frac{c_{44p} - c_{44m}}{\delta_{YINI} + \delta_{YISI}} \Big/ \left(\frac{c_{44p}}{\delta_{ZPI}} + \frac{c_{44m}}{\delta_{ZMI}}\right) \end{aligned} \tag{B.45}$$

$$\begin{aligned} w_I = {} & \left(w_P \frac{c_{33p}}{\delta_{ZPI}} + w_M \frac{c_{33m}}{\delta_{ZMI}}\right) \Big/ \left(\frac{c_{33p}}{\delta_{ZPI}} + \frac{c_{33m}}{\delta_{ZMI}}\right) \\ & - (u_{IE} - u_{IW}) \frac{c_{31p} - c_{31m}}{\delta_{XIEI} + \delta_{XIWI}} \Big/ \left(\frac{c_{33p}}{\delta_{ZPI}} + \frac{c_{33m}}{\delta_{ZMI}}\right) \\ & - (v_{IN} - v_{IS}) \frac{c_{32p} - c_{32m}}{\delta_{YINI} + \delta_{YISI}} \Big/ \left(\frac{c_{33p}}{\delta_{ZPI}} + \frac{c_{33m}}{\delta_{ZMI}}\right) \\ & + e_{33} E_z|_I \Big/ \left(\frac{c_{33p}}{\delta_{ZPI}} + \frac{c_{33m}}{\delta_{ZMI}}\right) \end{aligned} \tag{B.46}$$

$$v_{IN} = \frac{\delta_{ZPI}}{\delta_{ZMI} + \delta_{ZPI}} v_{MN} + \frac{\delta_{ZMI}}{\delta_{ZMI} + \delta_{ZPI}} v_{PN} \tag{B.47}$$

$$w_{IN} = w_I + \frac{\delta_{YINI}}{\delta_{YISI}}(w_I - w_{IS}) \tag{B.48}$$

$$v_{IS} = \frac{\delta_{ZPI}}{\delta_{ZMI} + \delta_{ZPI}} v_{MS} + \frac{\delta_{ZMI}}{\delta_{ZMI} + \delta_{ZPI}} v_{PS} \tag{B.49}$$

$$w_{IS} = w_I + \frac{\delta_{YISI}}{\delta_{YINI}}(w_I - w_{IN}) \tag{B.50}$$

$$P_1 = \frac{c_{11}}{\Delta x \rho}\left(\frac{1}{\delta_{XE}} + \frac{1}{\delta_{XW}}\right) + \frac{c_{66}}{\Delta y \rho}\left(\frac{1}{\delta_{YN}} + \frac{1}{\delta_{YS}}\right) + \frac{c_{55}}{\Delta z \rho}\left(\frac{1}{\delta_{ZF}} + \frac{1}{\delta_{ZR}}\right) \tag{B.51}$$

$$\varepsilon_1 = \frac{c_{11}}{\Delta x \rho \delta_{XE}} \tag{B.52}$$

$$W_1 = \frac{c_{11}}{\Delta x \rho \delta_{XW}} \tag{B.53}$$

$$N_1 = \frac{c_{66}}{\Delta y \rho \delta_{YN}} \tag{B.54}$$

$$S_1 = \frac{c_{66}}{\Delta y \rho \delta_{YS}} \tag{B.55}$$

$$F_1 = \frac{c_{55}}{\Delta z \rho \delta_{ZF}} \tag{B.56}$$

$$R_1 = \frac{c_{55}}{\Delta z \rho \delta_{ZR}} \tag{B.57}$$

$$B_{11} = \frac{c_{12}}{\Delta x \rho(\delta_{YN} + \delta_{YS})}\left(\frac{\delta_{XE} - \delta_{Xe}}{\delta_{XE}} - \frac{\delta_{XW} - \delta_{Xw}}{\delta_{XW}}\right) \tag{B.58}$$

$$B_{12} = \frac{c_{12}}{\Delta x \rho(\delta_{YENE} + \delta_{YESE})} \frac{\delta_{Xe}}{\delta_{XE}} \tag{B.59}$$

$$B_{13} = \frac{c_{12}}{\Delta x \rho(\delta_{YWNW} + \delta_{YWSW})} \frac{\delta_{Xw}}{\delta_{XW}} \tag{B.60}$$

$$B_{14} = \frac{c_{66}}{\Delta y \rho(\delta_{XE} + \delta_{XW})}\left(\frac{\delta_{YN} - \delta_{Yn}}{\delta_{YN}} - \frac{\delta_{YS} - \delta_{Ys}}{\delta_{YS}}\right) \tag{B.61}$$

$$B_{15} = \frac{c_{66}}{\Delta y \rho(\delta_{XNEN} + \delta_{XNWN})} \frac{\delta_{Yn}}{\delta_{YN}} \tag{B.62}$$

$$B_{16} = \frac{c_{66}}{\Delta y \rho(\delta_{XSES} + \delta_{XSWS})} \frac{\delta_{Ys}}{\delta_{YS}} \tag{B.63}$$

$$B_{17} = \frac{c_{13}}{\Delta x \rho(\delta_{ZF} + \delta_{ZR})}\left(\frac{\delta_{XE} - \delta_{Xe}}{\delta_{XE}} - \frac{\delta_{XW} - \delta_{Xw}}{\delta_{XW}}\right) \tag{B.64}$$

$$B_{18} = \frac{c_{13}}{\Delta x \rho(\delta_{ZEFE} + \delta_{ZERE})} \frac{\delta_{Xe}}{\delta_{XE}} \tag{B.65}$$

$$B_{19} = \frac{c_{13}}{\Delta x \rho(\delta_{ZWFW} + \delta_{ZWRW})} \frac{\delta_{Xw}}{\delta_{XW}} \tag{B.66}$$

$$B_{110} = \frac{c_{55}}{\Delta z \rho(\delta_{XE} + \delta_{XW})}\left(\frac{\delta_{ZF} - \delta_{Zf}}{\delta_{ZF}} - \frac{\delta_{ZR} - \delta_{Zr}}{\delta_{ZR}}\right) \tag{B.67}$$

$$B_{111} = \frac{c_{55}}{\Delta z \rho(\delta_{XFEF} + \delta_{XFWF})} \frac{\delta_{Zf}}{\delta_{ZF}} \tag{B.68}$$

$$B_{112} = \frac{c_{55}}{\Delta z \rho (\delta_{XRER} + \delta_{XRWR})} \frac{\delta_{Zr}}{\delta_{ZR}} \tag{B.69}$$

$$P_2 = \frac{c_{66}}{\Delta x \rho}\left(\frac{1}{\delta_{XE}} + \frac{1}{\delta_{XW}}\right) + \frac{c_{22}}{\Delta y \rho}\left(\frac{1}{\delta_{YN}} + \frac{1}{\delta_{YS}}\right) + \frac{c_{44}}{\Delta z \rho}\left(\frac{1}{\delta_{ZF}} + \frac{1}{\delta_{ZR}}\right) \tag{B.70}$$

$$\varepsilon_2 = \frac{c_{66}}{\Delta x \rho \delta_{XE}} \tag{B.71}$$

$$W_2 = \frac{c_{66}}{\Delta x \rho \delta_{XW}} \tag{B.72}$$

$$N_2 = \frac{c_{22}}{\Delta y \rho \delta_{YN}} \tag{B.73}$$

$$S_2 = \frac{c_{22}}{\Delta y \rho \delta_{YS}} \tag{B.74}$$

$$F_2 = \frac{c_{44}}{\Delta z \rho \delta_{ZF}} \tag{B.75}$$

$$R_2 = \frac{c_{44}}{\Delta z \rho \delta_{ZR}} \tag{B.76}$$

$$B_{21} = \frac{c_{66}}{\Delta x \rho (\delta_{YN} + \delta_{YS})}\left(\frac{\delta_{XE} - \delta_{Xe}}{\delta_{XE}} - \frac{\delta_{XW} - \delta_{Xw}}{\delta_{XW}}\right) \tag{B.77}$$

$$B_{22} = \frac{c_{66}}{\Delta x \rho (\delta_{YENE} + \delta_{YESE})} \frac{\delta_{Xe}}{\delta_{XE}} \tag{B.78}$$

$$B_{23} = \frac{c_{66}}{\Delta x \rho (\delta_{YWNW} + \delta_{YWSW})} \frac{\delta_{Xw}}{\delta_{XW}} \tag{B.79}$$

$$B_{24} = \frac{c_{21}}{\Delta y \rho (\delta_{XE} + \delta_{XW})}\left(\frac{\delta_{YN} - \delta_{Yn}}{\delta_{YN}} - \frac{\delta_{YS} - \delta_{Ys}}{\delta_{YS}}\right) \tag{B.80}$$

$$B_{25} = \frac{c_{21}}{\Delta y \rho (\delta_{XNEN} + \delta_{XNWN})} \frac{\delta_{Yn}}{\delta_{YN}} \tag{B.81}$$

$$B_{26} = \frac{c_{21}}{\Delta y \rho (\delta_{XSES} + \delta_{XSWS})} \frac{\delta_{Ys}}{\delta_{YS}} \tag{B.82}$$

$$B_{27} = \frac{c_{23}}{\Delta y \rho (\delta_{ZF} + \delta_{ZR})}\left(\frac{\delta_{YN} - \delta_{Yn}}{\delta_{YN}} - \frac{\delta_{YS} - \delta_{Ys}}{\delta_{YS}}\right) \tag{B.83}$$

$$B_{28} = \frac{c_{23}}{\Delta y \rho (\delta_{ZNFN} + \delta_{ZNRN})} \frac{\delta_{Yn}}{\delta_{YN}} \tag{B.84}$$

$$B_{29} = \frac{c_{23}}{\Delta y \rho (\delta_{ZSFS} + \delta_{ZSRS})} \frac{\delta_{Ys}}{\delta_{YS}} \tag{B.85}$$

$$B_{210} = \frac{c_{44}}{\Delta z \rho (\delta_{YN} + \delta_{YS})}\left(\frac{\delta_{ZF} - \delta_{Zf}}{\delta_{ZF}} - \frac{\delta_{ZR} - \delta_{Zr}}{\delta_{ZR}}\right) \tag{B.86}$$

$$B_{211} = \frac{c_{44}}{\Delta z \rho (\delta_{YFNF} + \delta_{YFSF})} \frac{\delta_{Zf}}{\delta_{ZF}} \tag{B.87}$$

$$B_{212} = \frac{c_{44}}{\Delta z \rho (\delta_{YRNR} + \delta_{YRSR})} \frac{\delta_{Zr}}{\delta_{ZR}} \tag{B.88}$$

$$P_3 = \frac{c_{55}}{\Delta x \rho}\left(\frac{1}{\delta_{XE}} + \frac{1}{\delta_{XW}}\right) + \frac{c_{44}}{\Delta y \rho}\left(\frac{1}{\delta_{YN}} + \frac{1}{\delta_{YS}}\right) + \frac{c_{33}}{\Delta z \rho}\left(\frac{1}{\delta_{ZF}} + \frac{1}{\delta_{ZR}}\right) \tag{B.89}$$

$$\varepsilon_3 = \frac{c_{55}}{\Delta x \rho \delta_{XE}} \tag{B.90}$$

$$W_3 = \frac{c_{55}}{\Delta x \rho \delta_{XW}} \tag{B.91}$$

$$N_3 = \frac{c_{44}}{\Delta y \rho \delta_{YN}} \tag{B.92}$$

$$S_3 = \frac{c_{44}}{\Delta y \rho \delta_{YS}} \tag{B.93}$$

$$F_3 = \frac{c_{33}}{\Delta z \rho \delta_{ZF}} \tag{B.94}$$

$$R_3 = \frac{c_{33}}{\Delta z \rho \delta_{ZR}} \tag{B.95}$$

$$B_{31} = \frac{c_{55}}{\Delta x \rho (\delta_{ZF} + \delta_{ZR})}\left(\frac{\delta_{XE} - \delta_{Xe}}{\delta_{XE}} - \frac{\delta_{XW} - \delta_{Xw}}{\delta_{XW}}\right) \tag{B.96}$$

$$B_{32} = \frac{c_{55}}{\Delta x \rho (\delta_{ZEFE} + \delta_{ZERE})} \frac{\delta_{Xe}}{\delta_{XE}} \tag{B.97}$$

$$B_{33} = \frac{c_{55}}{\Delta x \rho (\delta_{ZWFW} + \delta_{ZWRW})} \frac{\delta_{Xw}}{\delta_{XW}} \tag{B.98}$$

$$B_{34} = \frac{c_{31}}{\Delta z \rho (\delta_{XE} + \delta_{XW})}\left(\frac{\delta_{ZF} - \delta_{Zf}}{\delta_{ZF}} - \frac{\delta_{ZR} - \delta_{Zr}}{\delta_{ZR}}\right) \tag{B.99}$$

$$B_{35} = \frac{c_{31}}{\Delta z \rho (\delta_{XFEF} + \delta_{XFWF})} \frac{\delta_{Zf}}{\delta_{ZF}} \tag{B.100}$$

$$B_{36} = \frac{c_{31}}{\Delta z \rho (\delta_{XRER} + \delta_{XRWR})} \frac{\delta_{Zr}}{\delta_{ZR}} \tag{B.101}$$

$$B_{37} = \frac{c_{44}}{\Delta y \rho (\delta_{ZF} + \delta_{ZR})}\left(\frac{\delta_{YN} - \delta_{Yn}}{\delta_{YN}} - \frac{\delta_{YS} - \delta_{Ys}}{\delta_{YS}}\right) \tag{B.102}$$

$$B_{38} = \frac{c_{44}}{\Delta y \rho (\delta_{ZNFN} + \delta_{ZNRN})} \frac{\delta_{Yn}}{\delta_{YN}} \tag{B.103}$$

$$B_{39} = \frac{c_{44}}{\Delta y \rho (\delta_{ZSFS} + \delta_{ZSRS})} \frac{\delta_{Ys}}{\delta_{YS}} \tag{B.104}$$

$$B_{310} = \frac{c_{32}}{\Delta z \rho (\delta_{YN} + \delta_{YS})}\left(\frac{\delta_{ZF} - \delta_{Zf}}{\delta_{ZF}} - \frac{\delta_{ZR} - \delta_{Zr}}{\delta_{ZR}}\right) \tag{B.105}$$

$$B_{311} = \frac{c_{32}}{\Delta z \rho (\delta_{YFNF} + \delta_{YFSF})} \frac{\delta_{Zf}}{\delta_{ZF}} \tag{B.106}$$

$$B_{312} = \frac{c_{32}}{\Delta z \rho (\delta_{YRNR} + \delta_{YRSR})} \frac{\delta_{Zr}}{\delta_{ZR}} \tag{B.107}$$

$$A_{E1} = \frac{c_{12}}{c_{11}} \frac{\delta_{Xe}}{\delta_{YENE} + \delta_{YESE}} \tag{B.108}$$

$$A_{E2} = \frac{c_{13}}{c_{11}} \frac{\delta_{Xe}}{\delta_{ZEFE} + \delta_{ZERE}} \tag{B.109}$$

$$A_{E3} = \frac{e_{31}\delta_{XE}}{c_{11}} \tag{B.110}$$

$$A_{E4} = \frac{\delta_{Xe}}{\delta_{YENE} + \delta_{YESE}} \tag{B.111}$$

$$A_{E5} = \frac{\delta_{Xe}}{\delta_{ZEFE} + \delta_{ZERE}} \quad \text{(B.112)}$$

$$A_{W1} = \frac{c_{12}}{c_{11}} \frac{\delta_{Xw}}{\delta_{YWNW} + \delta_{YWSW}} \quad \text{(B.113)}$$

$$A_{W2} = \frac{c_{13}}{c_{11}} \frac{\delta_{Xw}}{\delta_{ZWFW} + \delta_{ZWRW}} \quad \text{(B.114)}$$

$$A_{W3} = \frac{e_{31}\delta_{XW}}{c_{11}} \quad \text{(B.115)}$$

$$A_{W4} = \frac{\delta_{Xw}}{\delta_{YWNW} + \delta_{YWSW}} \quad \text{(B.116)}$$

$$A_{W5} = \frac{\delta_{Xw}}{\delta_{ZWFW} + \delta_{ZWRW}} \quad \text{(B.117)}$$

$$A_{N1} = \frac{\delta_{Yn}}{\delta_{XNEN} + \delta_{XNWN}} \quad \text{(B.118)}$$

$$A_{N2} = \frac{c_{21}}{c_{22}} \frac{\delta_{Yn}}{\delta_{XNEN} + \delta_{XNWN}} \quad \text{(B.119)}$$

$$A_{N3} = \frac{c_{23}}{c_{22}} \frac{\delta_{Yn}}{\delta_{ZNFN} + \delta_{ZNRN}} \quad \text{(B.120)}$$

$$A_{N4} = \frac{e_{32}\delta_{YN}}{c_{22}} \quad \text{(B.121)}$$

$$A_{N5} = \frac{\delta_{Yn}}{\delta_{ZNFN} + \delta_{ZNRN}} \quad \text{(B.122)}$$

$$A_{S1} = \frac{\delta_{Ys}}{\delta_{XSES} + \delta_{XSWS}} \quad \text{(B.123)}$$

$$A_{S2} = \frac{c_{21}}{c_{22}} \frac{\delta_{Ys}}{\delta_{XSES} + \delta_{XSWS}} \quad \text{(B.124)}$$

$$A_{S3} = \frac{c_{23}}{c_{22}} \frac{\delta_{Ys}}{\delta_{ZSFS} + \delta_{ZSRS}} \quad \text{(B.125)}$$

$$A_{S4} = \frac{e_{32}\delta_{YS}}{c_{22}} \quad \text{(B.126)}$$

$$A_{S5} = \frac{\delta_{Ys}}{\delta_{ZSFS} + \delta_{ZSRS}} \quad \text{(B.127)}$$

$$A_{F1} = \frac{\delta_{Zf}}{\delta_{XFEF} + \delta_{XFWF}} \quad \text{(B.128)}$$

$$A_{F2} = \frac{\delta_{Zf}}{\delta_{YFNF} + \delta_{YFSF}} \quad \text{(B.129)}$$

$$A_{F3} = \frac{c_{31}}{c_{33}} \frac{\delta_{Zf}}{\delta_{XFEF} + \delta_{XFWF}} \quad \text{(B.130)}$$

$$A_{F4} = \frac{c_{32}}{c_{33}} \frac{\delta_{Zf}}{\delta_{YFNF} + \delta_{YFSF}} \quad \text{(B.131)}$$

$$A_{F5} = \frac{e_{33}\delta_{ZF}}{c_{33}} \quad \text{(B.132)}$$

$$A_{R1} = \frac{\delta_{Zr}}{\delta_{XRER} + \delta_{XRWR}} \quad \text{(B.133)}$$

$$A_{R2} = \frac{\delta_{Zr}}{\delta_{YRNR} + \delta_{YRSR}} \quad \text{(B.134)}$$

$$A_{R3} = \frac{c_{31}}{c_{33}} \frac{\delta_{Zr}}{\delta_{XRER} + \delta_{XRWR}} \quad \text{(B.135)}$$

$$A_{R4} = \frac{c_{32}}{c_{33}} \frac{\delta_{Zr}}{\delta_{YRNR} + \delta_{YRSR}} \quad \text{(B.136)}$$

$$A_{R5} = \frac{e_{33}\delta_{ZR}}{c_{33}} \quad \text{(B.137)}$$

References

[1] T. Sashida, T. Kenjo, An Introduction to Ultrasonic Motors, Oxford Science Publications, 1993.

[2] H. Hirata, S. Ueha, Characteristics estimation of a traveling-wave type ultrasonic motor, IEEE Transactions on Ultrasonics Ferroelectrics and Frequency Control 40 (4) (1993) 402–406, http://dx.doi.org/10.1109/58.251289.

[3] N. El Ghouti, Hybrid Modeling of Traveling Wave Piezoelectric Motor, Ph.D. thesis, Aalborg University, 2000.

[4] N. El Ghouti, J. Helbo, Equivalent circuit modeling of a rotary piezoelectric motor, in: IASTED International Conference on Modelling and Simulation (MS'2000), 2000.

[5] N.W. Hagood, A.J. McFarland, Modeling of a piezoelectric rotary ultrasonic motor, IEEE Transactions on Ultrasonics, Ferroelectrics, and Frequency Control 42 (1995) 210–224.

[6] J.L. Pons, H. Rodriguez, R. Ceres, L. Calderon, Novel modeling technique for the stator of traveling wave ultrasonic motors, IEEE Transations on Ultrasonics Ferroelectrics and Frequency Control 50 (11) (2003) 1429–1435, http://dx.doi.org/10.1109/TUFFC.2003.1251126.

[7] V. Bolborici, F.P. Dawson, M.C. Pugh, Modeling of composite piezoelectric structures with the finite volume method, IEEE Transactions on Ultrasonics, Ferroelectrics, and Frequency Control 59 (1) (2012) 156–162.

[8] V. Bolborici, Modeling of the Stator of Piezoelectric Traveling Wave Rotary Ultrasonic Motors, Ph.D. thesis, University of Toronto, 2009.

[9] V. Bolborici, F.P. Dawson, M.C. Pugh, Modeling of piezoelectric devices with the finite volume method, IEEE Transactions on Ultrasonics, Ferroelectrics, and Frequency Control 57 (7) (2010) 1673–1691.

[10] R.D. Mindlin, High frequency vibrations of piezoelectric crystal plates, International Journal of Solids and Structures 8 (1972) 895–906.

[11] COMSOL Material Libraries Module, COMSOL 4.3 Finite Element Software.